Direct dispersive signature of Pauli spin blockade with voltage bias

Simon Svab,[1,*] Rafael S. Eggli,[1,†] Taras Patlatiuk,[1] Miguel J. Carballido,[1] Pierre Chevalier Kwon,[1] Dominique A. Trüssel,[1] Ang Li,[2] Erik P.A.M. Bakkers,[2] Andreas V. Kuhlmann,[1] and Dominik M. Zumbühl[1,‡]

[1] *Department of Physics, University of Basel, Klingelbergstrasse 82, CH-4056 Basel, Switzerland*

[2] *Department of Applied Physics, TU Eindhoven, Den Dolech 2, 5612 AZ, Eindhoven, The Netherlands*

(Received 26 June 2025; revised 15 December 2025; accepted 21 January 2026; published 26 February 2026)

Pauli spin blockade (PSB) is a key paradigm in semiconductor nanostructures that gives access to the spin physics. We report the direct observation of PSB using gate-dispersive reflectometry on double quantum dots in the presence of a finite source-drain bias voltage. The reservoir charge transitions are strongly modulated, turning on and off when entering and leaving the blockaded region, consistent with a simple model. Observed in hole double quantum dots in a Ge/Si core/shell nanowire and a Si fin field-effect transistor, the effects are enhanced at larger bias voltage and suppressed by a magnetic field. This work establishes the fundamental dispersive signature of PSB under bias as an emerging tool for probing quantum dot devices.

DOI: 10.1103/8jmt-m432

I. INTRODUCTION

The exclusion principle proposed by Pauli [1] is a fundamental signature of quantum mechanics, ensuring proper symmetry of the wave function under particle exchange. In semiconductor nanostructures, this principle manifests as Pauli spin blockade (PSB) for fermions such as electrons [2] or holes [3]. PSB is both a fundamental paradigm of condensed-matter quantum statistics [4] and a key mechanism that has enabled high-fidelity spin readout in quantum dot systems. Since its first observation in the form of current rectification in a double quantum dot (DQD), caused by spin-selective tunneling due to the Pauli exclusion principle [2], the field of spin-based quantum computing [5] has progressed greatly. Compatibility with industrial semiconductor manufacturing processes has enabled promising scaling of qubit numbers in recent years [6–9], and isotopic purification of silicon has led to the realization of high-fidelity two-qubit gates [10].

These experimental demonstrations have crucially relied on PSB as an efficient mechanism for spin readout. Furthermore, PSB can be leveraged for qubit initialization, facilitating the operation and readout of qubits at elevated temperatures above 1 K [11–14], and even beyond liquid-helium temperatures [15]. While PSB provides the mapping of the quantum dot spin state to a more easily detectable charge state, the challenge of measuring this state with high fidelity and speed still remains.

An attractive method for direct *in situ* charge sensing is gate-dispersive reflectometry [16–21]. This requires no additional on-chip elements beyond the quantum dot gates and is also less invasive than sensing with an adjacent quantum dot, since random electron-tunneling fluctuations of the sensor dot induce back-action [22,23]. In particular, electrical modulations of the hole spin g factor [24,25] by nearby voltage fluctuations occurs monochromatically at the gate-sensor frequency, usually at a few 100 MHz, faster than the low-frequency noise responsible for dephasing as well as sensor back-action-induced infidelities [23]. This can also be seen by the fact that phase driving [25] is observed below 15 MHz. Additionally, typical gate sensors apply signal amplitudes of the order of μV [18,26,27], much lower than the mV qubit drive amplitudes [15,28,29], which further highlights the low invasiveness of dispersive gate sensing.

Using gate reflectometry, the quantum capacitance of a given charge state can be probed at the interdot transition, providing information on the energy-level diagram, as it is proportional to the curvature of the energy level with respect to the probe gate voltage [17,30]. This allows resolution of anticrossings in a DQD energy-level diagram originating from tunnel coupling and other off-diagonal terms in the Hamiltonian of the system; however, directly detecting PSB in gate-sensing experiments can prove challenging, as large magnetic fields are required [31] and nonreciprocities are encountered depending on the detailed system parameters [32]. Furthermore, strong

*Contact author: simon.svab@unibas.ch

†This author contributed equally to this work as the first author.

‡Contact author: dominik.zumbuhl@unibas.ch

spin-orbit interaction and highly variable site-dependent and anisotropic g tensors, as present in hole spin systems in Si [24,33] and Ge [34,35], further complicate the two-spin level diagram, resulting in highly variable dispersive signatures of PSB. This is particularly relevant for hole devices with strong biaxial confinement, such as Ge/Si core/shell nanowires (NWs) [36–39] and Si fin field-effect transistors (FinFETs) [15,40], which are the two platforms we will focus on in what follows. We note that the dispersive feature of PSB described here is expected to be equally present for electrons and in other materials systems.

Crucially, previous reports that dispersively sensed spin-blocked DQDs did not investigate the dispersive signature of current rectification due to PSB, as they operated at zero source-drain bias. Instead, the magnetic-field evolution of the dispersively sensed interdot charge transition [18,20,30,31,41] or suppression of the reservoir transition by spin latching [19] were extensively studied. In light of its fundamental and technological relevance, investigating the dispersive signature of PSB under bias, and thereby understanding the dispersive manifestation of the canonical transport rectification [2], presents a still largely uncharted area in semiconductor quantum dot physics and spin-based quantum information.

Here, we fill this gap in the literature by presenting the dispersive signatures of the PSB in a Ge/Si core/shell NW DQD [36–39] using radio-frequency (rf) reflectometry at finite bias voltage and compare it to the dc signal. The dispersive signal of the reservoir transitions is strongly modulated by PSB: at the upper triple point, the dispersive signal is suppressed in the leaking and enhanced in the blockaded regime, strongly alternating its magnitude. At the other triple point, this pattern is reversed, while the dc transport looks very similar at both triple points. In a magnetic field, we observe the simultaneous lifting of PSB both in the dc transport and in the gate-dispersive signal. These results establish gate-dispersive sensing of PSB under voltage bias as an alternative route for probing the intricate spin physics in DQDs.

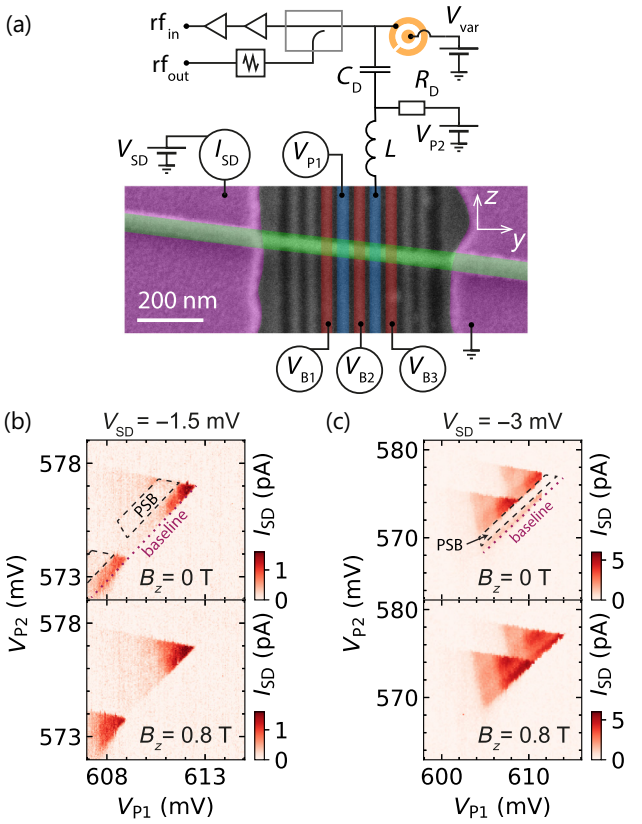

FIG. 1. PSB in a Ge/Si NW DQD. (a) False-colored scanning electron micrograph of a Ge/Si NW device similar to the one used in the experiment (NW angle and curvature may differ slightly). The reflectometry is connected to the right-hand plunger gate for dispersive sensing, impedance matched with the varactor shown in orange (see Ref. [26] for details). Measured dc signal I_{SD} at source-drain bias (b) $V_{SD} = -1.5$ mV and (c) $V_{SD} = -3$ mV. The baselines of the triangles at $B_z = 0$ T are indicated by purple dotted lines, and the regions where current is suppressed due to PSB are shown by dashed black boxes. The magnetic field lifts the blockade, resulting in an increase of I_{SD} in the PSB region. The abrupt disappearance of current in the upper-right corner of the triangle at $V_{SD} = -3$ mV and $B_z = 0$ T is due to a random charge switcher.

II. RESULTS

A. PSB in a hole DQD

The experimental setup, including the NW device [36–39] used in this work, is depicted in Fig. 1(a). More details on the device and setup can be found in Ref. [26]. These NWs can host highly tunable and repeatable hole quantum dots [42–45], and the strong, electrically tunable direct Rashba spin-orbit interaction arising from the heavy-hole–light-hole mixing [46,47] can be harnessed to achieve fast, all-electrical spin control that is compatible with dispersive gate sensing [29]. We furthermore observe high gate lever arms of up to 0.4 in these devices, which facilitates charge sensing through device gates [26,48].

We form a DQD by applying positive voltages to five of the nine bottom gates [indicated in Fig. 1(a)], locally depleting the hole gas in the NW. The barrier gates (red, at $V_{B1,B2,B3}$) are operated at more positive voltages, creating appropriate tunneling rates, while the plunger gates (blue, at $V_{P1,P2}$) control the hole occupation. The right-hand plunger gate is connected to further circuitry, including a surface-mount ceramic-core inductor, a bias tee, and a voltage-tunable capacitor made of strontium titanate [26,49]. The dispersive gate sensor operates at $f_0 \simeq 316.2$ MHz with a loaded quality factor $Q \simeq 52$ [26]. The NW is contacted on both ends, allowing for simultaneous measurements of the direct current I_{SD} and the gate-dispersive signal, which is demodulated

to give an amplitude and a phase component. Throughout this paper, we define the reflected phase away from the charge transitions as $\phi = 0^\circ$ and display the modulus phase change ϕ.

At a finite source-drain bias voltage V_{SD}, scanning the plunger gates V_{P1} and V_{P2} against each other and measuring the dc signal reveals bias triangles, the characteristic signature of a DQD, as shown in Figs. 1(b) and 1(c). The charge-stability map [26] indicates typical addition energies of $E_{add} \simeq 6$ meV and orbital splittings around $E_{orb} \simeq 0.6$ meV for this particular DQD configuration, slightly lower than previous reports from similar devices operated in the same gate configuration [14,39,50].

We observe the characteristic dc signature of PSB in the presence of strong spin-orbit mixing [14,35,40,51]. In the spin-blocked transport direction with a negative bias voltage V_{SD} applied, transport current $|I_{SD}|$ is suppressed by PSB in a region [black dashed boxes in Figs. 1(b) and 1(c), upper panels] close to the triangle baseline. When a magnetic field B is applied, $|I_{SD}|$ increases in the PSB region [see Figs. 1(b) and 1(c), lower panels]. This is due to coupling of the spin-blockaded triplet states to the singlet state when the magnetic field is turned on, thereby lifting the PSB [51,52].

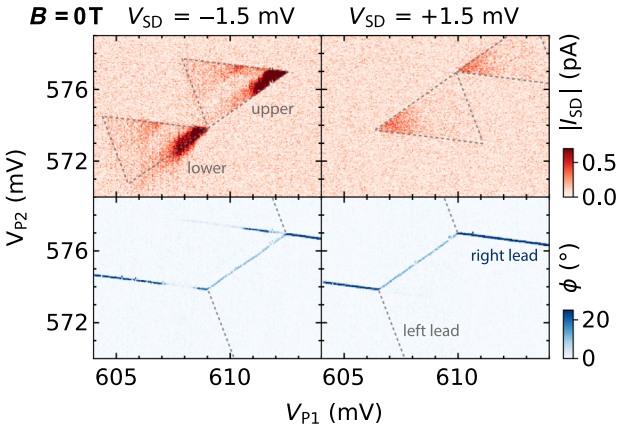

FIG. 2. Dispersive signature of PSB. Simultaneously measured dc signal $|I_{SD}|$ (top) and reflected phase ϕ (bottom) in the PSB configuration, shown for $V_{SD} = \pm 1.5$ mV and $B = 0$ T. In the dc data, the upper and lower bias triangles are indicated by dashed outlines and the dispersively sensed right-lead transition is labeled, while the position of the (invisible) left reservoir transition is indicated by dashed grey lines. The dispersive signature of PSB is revealed in the right-lead transition, which shows a peculiar pattern of turning on (off) at the upper (lower) bias triangle for $V_{SD} = -1.5$ mV. At $V_{SD} = +1.5$ mV, the dispersive charge-stability map is unaffected by PSB, thus following the standard honeycomb pattern.

B. Dispersive signature of PSB

Having established the presence of PSB in our DQD for negative V_{SD}, Fig. 2 compares the dc signal (upper panels) with the dispersively measured phase ϕ of the reflected rf signal (lower panels) for $V_{SD} = \pm 1.5$ mV. We note two different types of transitions in the dispersive data: interdot transitions correspond to tunneling events between the two quantum dots and trace the baseline of a bias triangle, extending diagonally from lower left to upper right. The lead transitions, in contrast, follow the other flanks of the bias triangles. Here, we see only the right-lead transitions since the right-hand plunger gate P2 (plunging the right-hand dot) is connected to the reflectometry. This detects the tunneling between the right-hand quantum dot and its adjacent reservoir. Note the qualitatively different behavior of the right-lead transition for (the spin-blocked) $V_{SD} = -1.5$ mV compared to the opposite (spin-unblocked) $V_{SD} = +1.5$ mV. The visibility modulations of the right-lead transition for the spin-blocked bias direction constitute the dispersive signature of PSB, which will be the object of study for the remainder of this work. The expected position of the invisible left-lead transition is indicated with dashed grey lines in the dispersive data. The direct correspondence of I_{SD} and ϕ is confirmed in Fig. 3(a), where the data are superimposed.

First, it is worth pointing out a few subtleties of the dc data shown in Figs. 2 and 3(a). Inside the upper triangle, and along the upper-lead transition for negative bias, there is a band of weak current. We assign this effect to reservoir exchange partially lifting the blockade [53,54]. Another effect is a band of current starting from the zero-detuning line inside the triangle. The size of this band changes with the interdot tunneling strength (see Appendix B) and is caused by some mechanism lifting the PSB, presumably due to spin-flip cotunneling [55–57]. In this band, the current increases when approaching the upper flank of the bias triangles, consistent with cotunneling [56] and suggesting asymmetric reservoir tunneling rates, here with a stronger coupling to the right-hand reservoir. The width of this feature could be related to the exchange splitting J. This appears in numerous places in the current; see Ref. [58], where bias effects were considered, albeit not along the detuning axis. Finally, we note that there are lines, parallel to the left-lead transitions, at which the current changes. This can be explained with (ground and excited) states of the left-hand QD being aligned with the Fermi level of the left-hand reservoir [59].

Next, we take a closer look at the lead transitions in reflectometry. Each QD contains dozens of holes, but for the case of PSB, the effective charge states correspond to those indicated by "(m, n)" in Fig. 3(a), where m (n) denotes the number of excess holes in the left-hand (right-hand) dot. The energy-level diagrams for some representative configurations (indicated with colored markers) are drawn in Fig. 3(b). The "$(1, 0)$" $\leftrightarrow$ "$(1, 1)$" lead transition (orange square) corresponds to the "$(1, 1)$" energy level of the right-hand QD being aligned with the Fermi level of the

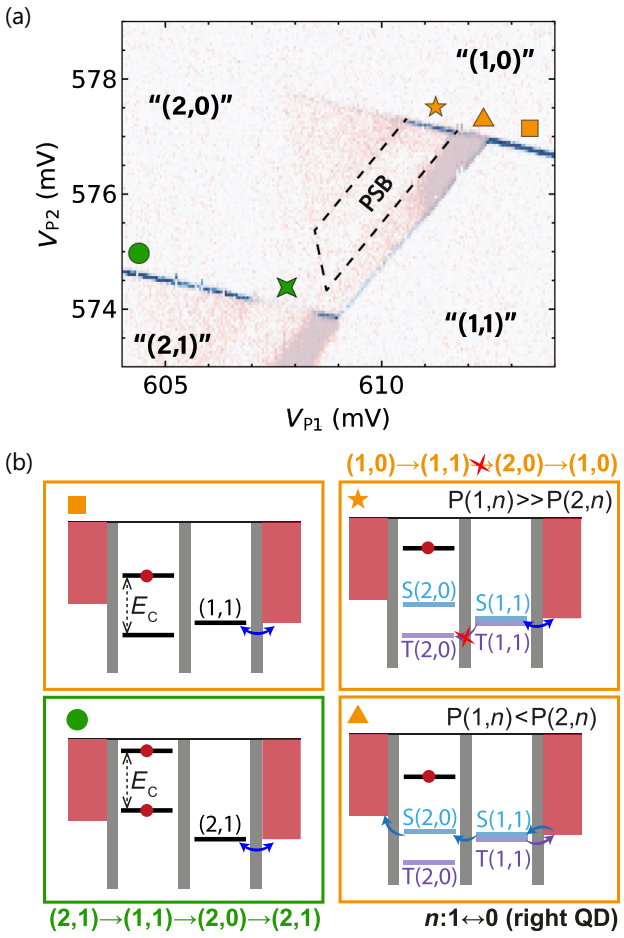

FIG. 3. Phenomenological model. (a) Enlarged view of the scan at $V_{SD} = -1.5$ mV, with superimposed $|I_{SD}|$ (red color scale) and ϕ (blue color scale). Effective charge occupations are labeled. The region between the dashed lines demarcates the PSB area with suppressed current in the upper triangle. The two lead transitions show complementary but opposite dispersive signatures between the upper- and lower-lead transitions (see star and triangle regions). This is consistent with the PSB mechanism affecting the transport cycles (see main text). (b) Schematic illustration of the DQD energy levels and the relevant transport cycles shown for different points along the lead transitions, as indicated in (a). In a band close to zero detuning (orange triangle), PSB is lifted and a weak leakage current flows, presumably due to spin-flip cotunneling.

right-hand reservoir. This leads to resonant tunneling with the reservoir (blue arrow) and a change of the right-hand QD charge state as this line is crossed. The corresponding change of the dot level population appears in the tunneling capacitance and is picked up by the reflectometry [60]. When the energy levels of the left-hand QD lie outside the bias window, there is no dc transport through the DQD due to Coulomb blockade, while a finite ϕ can be measured on the lead transition.

Inside the dashed lines in Fig. 3(a), PSB causes the DQD to remain stuck in the T(1,1) state for most of the time, such that the measured $|I_{SD}|$ is very low. Transport can occur at a large enough detuning where the T(2,0) state becomes energetically accessible. At low detuning, PSB is lifted by some process such as cotunneling, providing a band of current from the zero detuning up to the dashed line. Finally, there can also be reservoir exchange along the upper edge of the bias triangle. In the presence of PSB leakage, resonant tunneling with the right-hand reservoir is suppressed due to the slow left-hand reservoir tunneling. This keeps the right-hand dot in the 0 state for most of the time, and thus the change of population across the reservoir line is weak, as seen by the almost completely suppressed gap in the dispersive sensing at the orange triangle. In contrast, the dispersive signal is high in the spin-blockaded region (orange star), although not quite as strong as in the Coulomb blockade region (orange square). To check the important role of the asymmetric DQD setup as hypothesized above, we increase the left-hand dot tunneling rate and observe that the dispersive signal indeed recovers in strength, as expected; see Appendix C.

Shifting the focus to the "(2, 0)" ↔ "(2, 1)" lead transition (green circle), this is the case of two holes on the left-hand dot, while the energy level of the right-hand QD is still aligned with the Fermi level of the right-hand reservoir. In analogy to the orange square region, but now with two holes on the left-hand dot, the "(2, 0)" ↔ "(2, 1)" transition produces a change in the charge state of the right-hand QD, leading to a change in the tunneling capacitance. We note that this transition traces the other bias triangle, whose transport cycle is different—namely, the occupation in the DQD is cycling between "2" ↔ "3" holes instead of "1" ↔ "2", as labeled in Fig. 3(b). Nonetheless, the transport cycle involves an occupation where the DQD can get stuck in the T(1,1) state due to PSB, leading to a reduced $|I_{SD}|$ and a suppression of right-hand reservoir tunneling, thus turning off the tunneling capacitance and phase signal; see the gap in the lower reservoir transition (green star).

We note that the dispersive signals at the edges of the two triangles are complementary and opposite in behavior: for example, at the starred regions (orange and green stars), the PSB is mostly intact and keeps the DQD blocked in the T(1,1) state for most of the time. At the upper triangle (orange star), the reservoir transition "(1, 1)" ↔ "(1, 0)" remains active, with resonant tunneling with the reservoir ongoing, producing a strong dispersive signal. Conversely, at the lower transition (green star), the occupation of the $T(1, 1)$ in PSB mostly deactivates the right-hand reservoir transition "(2, 1)" ↔ "(2, 0)", giving a weak dispersive signal, as indeed seen in the data.

Similar signatures of dispersive PSB were also observed in a Si FinFET hole spin qubit device, now with absolute hole numbers one and two (see Appendix D). The dispersive gap at the upper reservoir transition is present, along with the reappearance of the dispersive signal when PSB is intact, and its mirror image at the lower

reservoir. The dispersive gap is perhaps slightly weaker or smaller, but this also depends on the interdot tunneling (see Appendix A) as well as the left-hand dot rate (see Appendix C). Thus, this confirms the same key signatures in a different material and device type. Note that the FinFET has a sensor gate lever arm of approximately 0.05 [29], similar to planar qubit device platforms [12,61], suggesting that the dispersive PSB signature can be found in most common device architectures.

We now aim to provide a phenomenological explanation for our observation. The measured change in ϕ is proportional to the parametric capacitance $C_{\mathrm{PM}} = C_Q + C_{\mathrm{TU}}$, where C_Q is the quantum capacitance due to the curvature of the (occupied) energy levels, i.e., from the singlet-triplet anticrossing. The tunneling capacitance C_{TU} [62] can be written as [32,63]

$$C_{\mathrm{TU}} = (e\alpha)^2 \sum_i \left(\frac{1}{2} \left(1 + 2\frac{\partial E_i}{\partial \varepsilon} \right) \frac{\partial P_i}{\partial \varepsilon} \right), \qquad (1)$$

where α is the gate lever arm, P_i the occupation probability of each individual state with energy E_i, and ε is the DQD detuning. This equation takes into account the change of the dot occupations and the slope of the energy levels, and it only considers the internal DQD transition. A similar term applies to the lead transitions. The occupations change in a steplike manner at the charge transitions, where a large C_{TU} results for both the interdot and lead transitions. Further, PSB influences the populations, in particular leading to a reappearance of the reservoir line at the orange star in the blockaded regime, and conversely a suppression at the green star in Fig. 3(a). The quantum capacitance is visible near zero detuning in our dataset, where the curvature of the DQD anticrossing appears, and this contributes no significant signal to the lead transitions.

C. Dependence on experimental parameters

We further investigate the conditions under which the described dispersive signature is modulated. In Fig. 4(a), we show an enlarged view of the "(2, 0)" ↔ "(2, 1)" lead transition for two different V_{SD} values, as labeled. While the strength of the lead transition is essentially constant at zero bias, the dip in the lead signal emerges for more negative voltage bias. We perform line cuts along the lead transition, as indicated with colored dashed lines, and obtain the profiles shown in Fig. 4(b). For negative bias, the dispersive gap (shaded gray) appears in the PSB region, ultimately approaching the background value, corresponding to the absence of reservoir tunneling. This is reminiscent of the original observation of PSB [2], where the blockaded region in direct current appeared only at bias voltages above which the triplet becomes available. Similarly, the phase signal weakens in the region between the gap and zero detuning as the dispersive gap saturates.

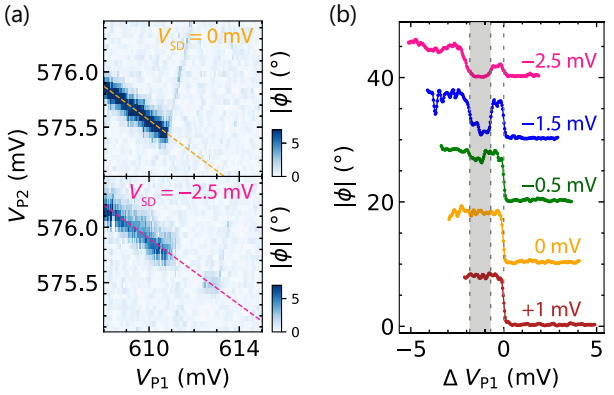

FIG. 4. Bias dependence. (a) Dispersive phase shift $|\phi|$ at the "(2, 0)" ↔ "(2, 1)" lead transition, shown at $B = 0$ T. Colored dashed lines indicate the line cuts shown in (b) along the lead transition for bias voltages as labeled. These line cuts are obtained by interpolation and smoothing. The zero-detuning flank defines the zero of the axis. The gray shading demarcates the region in which the DQD is mostly in T(1,1). As V_{SD} becomes more negative, the suppression of $|\phi|$ due to PSB becomes visible (gray area) and also decreases in the cotunneling region, from the edge of the gray band to zero detuning.

These effects illustrate how C_{TU} can change inside the bias window.

Additionally, the dispersive feature depends on the strength of the applied magnetic field. As highlighted in Fig. 5(a), the dispersive gap is filled in and the dispersive

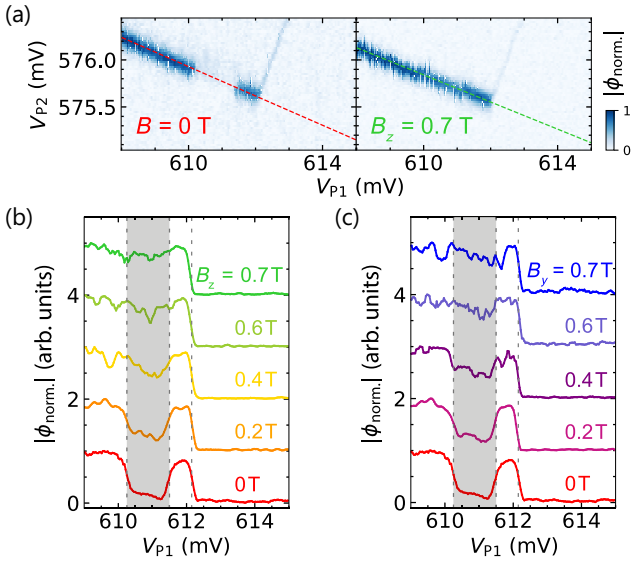

FIG. 5. B-field dependence. (a) Normalized phase at the (2, 0) ↔ (2, 1) lead transition at $V_{\mathrm{SD}} = -1.5$ mV and magnetic fields as labeled. Colored dashed lines indicate the line cuts shown in (b),(c), where the magnetic-field evolution is shown as labeled. The z axis is in plane and perpendicular to the NW, and the y axis is essentially along the NW. With increasing field, the visibility of the dispersive gap (gray bar) is restored, similarly for B fields along the y or z axes.

signal is restored when the magnetic field is increased. This is in line with the dc characteristics in this charge configuration (see Appendix A). Next to the lead transition, one can also see in Fig. 5(a) that the interdot transition becomes weaker in presence of a B field, similar to previous reports [18,20,64,65]. Finally, we note the slightly noisier data in the presence of a magnetic field, indicating elevated switching noise, possibly more pronounced for the y field. This could be due to a somewhat elevated temperature or B-field-induced shifts of the two-level fluctuators.

III. CONCLUSIONS AND OUTLOOK

We have observed the dispersive signatures of PSB in a DQD at finite bias. Asymmetric reservoir coupling boosts the visibility of the dispersive signal at the reservoir transition, where the dispersive signal switches on and off together with the PSB current. Similar signatures were also observed in a Si FinFET device. A first phenomenological model is consistent with the dispersive PSB signals, but more work is needed for a quantitative understanding, particularly of the leakage current. This may be complicated by the fact that the DQD operates with holes and experiences strong spin-orbit coupling.

The minimally invasive gate reflectometry allows for short integration times, thus providing access to time-resolved spin physics [30]. We note that the exact same setup and NW device has reached charge readout at μs timescales [26] on the reservoir transition, thus potentially allowing fast spin readout at similar speeds using the outlined dispersive signature of PSB. Note that adding a quantum-limited low-noise amplifier at the mK stage could further reduce the readout times [60,66]. The performance of this approach requires further validation in future experiments, thereby adding a largely unexplored operation modality to the repertoire of spin-readout approaches. Here, effects that lift PSB, such as spin-flip cotunneling, could reduce readout fidelity; however, note that we were able to tune the extent to which this effect was present in our experiment (Appendix B), and this limitation applies to all PSB-based readout methods.

Furthermore, our method may provide access to the study of spin physics of biased DQDs, and associated nonreciprocities [32], anisotropies [33,34], back-action effects [22,23], and spin-orbit coupling [51]. It is important to note that a finite source-drain bias is required to observe the dispersive PSB feature we describe. Additionally, reservoir tunneling must be possible at tunnel rates close to the readout resonator frequency [30], ruling out QDs operated in isolated mode [10,11] from using our method. Our observation of the dispersive PSB feature with the FinFET (Appendix D) demonstrates that these conditions on reservoir tunnel rate and bias can be satisfied in the single-particle regime, which is often desired for spin-qubit experiments [6,7,18]. On the other hand, the many-hole regime in which our NW experiments were performed still readily accommodates qubit operation [13–15,61] and enables the study of many-particle spin states [21].

ACKNOWLEDGMENTS

We thank S. Bosco, W.A. Coish, E.R. Franco Diaz, and J.C. Egues for useful theory discussions. Further thanks go to A. Efimov and Y. Liu for additional experimental efforts in the Ge/Si NW project, and to E. Kelly, A. Orekhov, and G. Salis for providing the superconducting nanowire inductors used in the experiments with the FinFET device. Furthermore, we acknowledge S. Martin and M. Steinacher for technical support. This work was partially supported by the Swiss Nanoscience Institute (SNI), the NCCR SPIN, the Georg H. Endress Foundation, Swiss NSF (Grant No. 179024), the EU H2020 European Microkelvin Platform EMP (Grant No. 824109), and FET TOPSQUAD (Grant No. 862046).

S.S., R.S.E., and D.M.Z. conceived of the project and planned the experiments. S.S. fabricated the NW device with contributions from M.J.C. and P.C.K. S.S. performed the experiments on the Ge/Si NW with inputs from R.S.E. and T.P. S.S. and R.S.E. outlined the phenomenological explanation of the dispersive signature with inputs from D.M.Z. R.S.E. performed the experiments with the FinFET device, which was fabricated by A.V.K. T.P. and D.A.T. contributed to the experimental setup. S.S. analyzed the data with inputs from R.S.E., T.P., and D.M.Z. A.L. grew the NWs under the supervision of E.P.A.M.B. S.S. wrote the manuscript with inputs from all authors. D.M.Z. supervised the project.

DATA AVAILABILITY

The data that support the findings of this article are openly available [67].

APPENDIX A: DC SCANS

Here, we provide additional information on the data presented in the main text. As a standard configuration, the DQD was operated at barrier-gate voltages $V_{B1} = 2$ V, $V_{B2} = 1.82$ V, and $V_{B3} = 3$ V. We note that all scans were performed by ramping from negative to positive voltages, and that V_{P1} is the slow axis while V_{P2} is the fast axis.

Interestingly, at an increased bias-window size, the transport would occasionally become blockaded in the region close to the corner [adjacent to the baseline and the $(1,0) \leftrightarrow (1,1)$ lead transition] of the upper triangle at $B = 0$ T, leading to a seemingly missing section of the bias triangle shown in the upper panel of Fig. 1(c) in the main text. Scanning V_{P2} through this region with a high resolution (i.e., a longer time spent in this region), we note that dc transport through the DQD seemed to become blocked and unblocked every now and then (on the timescale of few

tens of seconds). A scan in the same gate configuration (measured several weeks later, after investigating other gate configurations) is presented in Fig. 6(a) (rightmost panel), showing that these data were well reproducible within the same thermal cycle.

APPENDIX B: WIDTH OF THE CURRENT BAND NEAR ZERO DETUNING

In the main text, we found that PSB is lifted in a band close to zero detuning, which may, for example, originate from inelastic (spin-flip) cotunneling [55–57]. Here, we show that the width of this band depends on the center barrier-gate voltage V_{B2}, and hence the interdot tunneling rate. In Fig. 6(a), we present further scans of the bias triangles presented in the main text, taken at different values of V_{B2}. Qualitatively, it can be seen that the width of the band is narrower at $V_{B2} = 1.805$ V than at the two other barrier-gate configurations. We confirm this quantitatively by performing nearest-neighbor interpolation of the data through the indicated axes, yielding the line cuts as shown in Fig. 6(b). To better distinguish the narrow peak widths, we do not perform any smoothing on these line cuts. We extract $\delta\varepsilon_{\mathrm{cot}}$ as the mean value of the full width at half maximum averaged over ten adjacent collinear line cuts, and we plot the values in Fig. 6(c), along with the standard deviations as error bars. In our data, we find that $\delta\varepsilon_{\mathrm{cot}}$ is halved within this range of V_{B2}, with a local minimum at $V_{B2} = 1.81$ V.

In the spin-flip cotunneling theory, the dependence of $\delta\varepsilon_{\mathrm{cot}}$ on V_{B2} could be explained by considering the tunneling rates involved and following Refs. [55–57], such that the cotunneling peak width $\delta\varepsilon_{\mathrm{cot}}$ at $B = 0$ is expressed as

$$\delta\varepsilon_{\mathrm{cot}} = \left(\frac{3\Gamma_S t^2}{W^0_{\mathrm{cot}}}\right)^{1/2}. \tag{B1}$$

Here, W^0_{cot} is the spin-flip cotunneling rate, given by

$$W^0_{\mathrm{cot}} = \frac{k_B T}{\pi\hbar}\left[\left(\frac{\hbar\Gamma_D}{\Delta-\varepsilon}\right)^2 + \left(\frac{\hbar\Gamma_S}{\Delta+\varepsilon-2U_{lr}-2|eV_{\mathrm{SD}}|}\right)^2\right], \tag{B2}$$

where Δ sets the energy of the $(1,1)$ charge configuration and U_{lr} is the mutual (interdot) charging energy. Taking $\Gamma_S \ll \Gamma_D$ for the source (drain) lead tunneling rates, as is also valid for our data, the expression for the cotunneling rate becomes

$$W^0_{\mathrm{cot}} \simeq \frac{k_B T}{\pi\hbar}\left(\frac{\hbar\Gamma_D}{\Delta-\varepsilon}\right)^2. \tag{B3}$$

Inserting this back into Eq. (B1) yields

$$\delta\varepsilon \propto \frac{\sqrt{\Gamma_S}}{\Gamma_D} t. \tag{B4}$$

Thus, one can see that $\delta\varepsilon$ is influenced by all three tunneling rates of the DQD system. Circling back to our data in Fig. 6(c), and considering that the tunneling rates in our depletion-mode hole DQD decrease as gate voltages become more positive, we argue that $\delta\varepsilon$ decreases from $V_{B2} = 1.79$ to 1.81 V as a consequence of the simultaneously decreasing interdot tunneling rate, t.

From $V_{B2} = 1.81$ to 1.82 V, the extracted $\delta\varepsilon$ increases again. Since t should continue to be suppressed more by V_{B2}, this hints at the ratio of reservoir tunneling rates $\sqrt{\Gamma_S}/\Gamma_D$ rising in this interval, thereby increasing $\delta\varepsilon$. Indeed, a closer look at the plunger-gate voltage values in Fig. 6(c) shows that the negative compensation of V_{P1} (as V_{B2} becomes more positive) is approximately double that of V_{P2}. Thus, we reason that these plunger gates

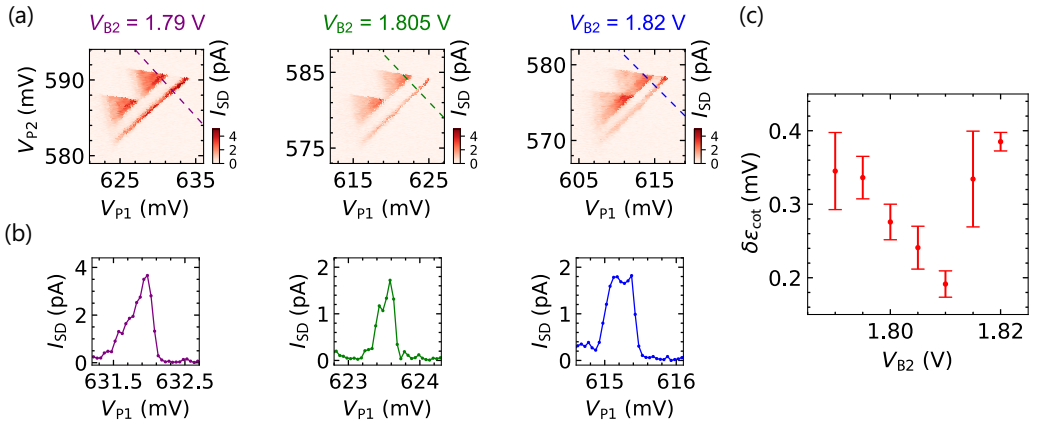

FIG. 6. Width of the current band. (a) Plots of dc measurements of the investigated pair of bias triangles, shown for different interdot barrier-gate voltages V_{B2}. Data in the main text were taken at $V_{B2} = 1.82$ V. (b) Line cuts through the indicated axes in (a), allowing extraction of the peak width $\varepsilon_{\mathrm{cot}}$. (c) Extracted $\varepsilon_{\mathrm{cot}}$ as a function of V_{B2}. The error bars correspond to the standard deviation of peak widths obtained from line cuts close to the region of interest.

affect their adjacent reservoir tunneling barriers, Γ_S and Γ_D, respectively, and that Γ_S is rising more strongly in this gate-voltage range, leading to an increase in $\sqrt{\Gamma_S}/\Gamma_D$ and thus a broader $\delta\varepsilon$.

APPENDIX C: LEFT-BARRIER-GATE DEPENDENCE

In our experiment, we have also observed that the modulation strength of the sensing signal along the bias triangle changes as one tunes the left-barrier-gate voltage V_{B1} (corresponding to the source tunneling rate Γ_S). This can be seen in the dataset in Fig. 7, taken in the same bias triangle as the one shown in the main text, albeit at a later point in time after retuning the device to this voltage configuration. As V_{B1} is increased, we see that the change in contrast (of the dispersive signal) along the lead transition becomes pronounced. As we argue in the main text, this may stem from changes in the transport cycle, leading to larger differences in $\partial P_i/\partial\epsilon$ in the different sectors of the bias triangle.

APPENDIX D: ADDITIONAL DATA FROM A Si FINFET DQD

We have found similar dispersive PSB features in a Si FinFET device [15,33,40], which was cooled in the same dilution refrigerator but using a superconducting NbN nanowire inductor [29,68] in the tank circuit. The tank was attached to the right-hand plunger gate. For a detailed description of the device, see Ref. [29]. Note that the identical device and charge transition was used in previous works [25,29] to perform spin-qubit experiments using dc-based spin readout [15]. From the absence of further transitions in larger-scale charge-stability maps (not shown), we conclude that the DQD's absolute charge occupation was $(1,1) \leftrightarrow (2,0)$. The correspondence of the data taken with the FinFET to the results in the main text is highlighted in Fig. 8. The $(1,1) \leftrightarrow (2,0)$ charge transition at relatively small bias $V_{SD} = -1$ mV (we use the same convention for the bias sign as for the NW) is depicted in Fig. 8(a), where the reservoir transition shows segments similar to the data presented in Fig. 3(a). The corresponding segments are marked analogously, highlighting in the upper reservoir transition the $(1,1) \leftrightarrow (1,0)$ transition outside of the bias window (orange circle), the gap due to PSB lifting close to zero detuning [orange triangle in the enlarged view in Fig. 8(b)], and the bright PSB regime in the upper reservoir transition (orange star). In the lower reservoir transition, the PSB regime shows low visibility (green star), and the transition is recovered outside the bias window where the $(2,0) \leftrightarrow (2,1)$ (orange circle) reappears. Note the absence [compared to Fig. 3(a)] of the high-visibility feature close to zero detuning in the lower reservoir transition, presumably due to a different imbalance of the reservoir tunnel rates as compared to the NW DQD. Because the FinFET device only featured one dedicated interdot barrier gate, which was set to $V_B = -930$ mV for all displayed experiments, the reservoir tunnel rates were only poorly tuneable and the impact of the imbalance in the reservoir tunnel rate could not be further studied.

An interesting side note is the visibility of the interdot transition along the triangle baselines. Due to a relatively large mutual capacitance, the triple points are separated in energy by a sufficient amount that the triangles do not overlap for $V_{SD} = -1$ mV. The interdot transition is therefore partially present outside (light blue arrow) and inside

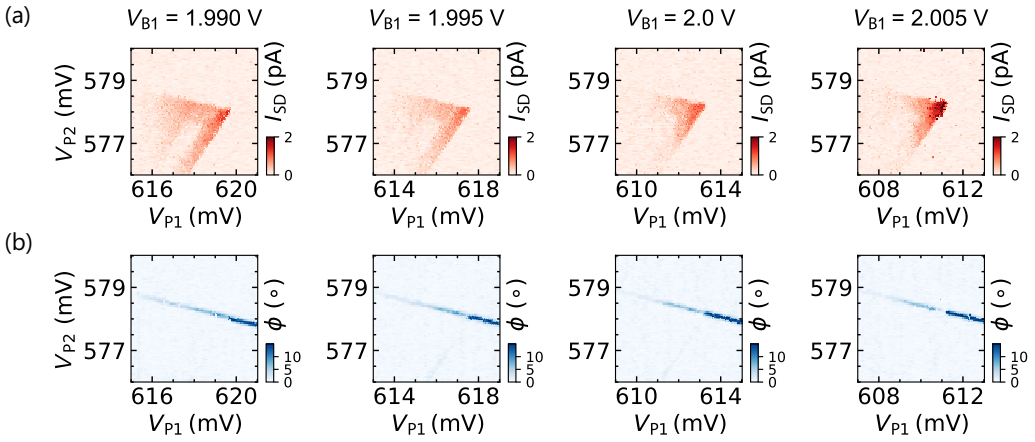

FIG. 7. Dependence on the left barrier-gate voltage. (a) Measured dc signal and (b) corresponding dispersive signal ϕ of the investigated pair of bias triangles, shown for different left-barrier-gate voltages V_{B1}. The gap of the dispersive signal (right-hand panel, lowest left-hand dot tunneling rate) along the reservoir transition closes and the dispersive signal is recovered as the left-hand dot tunneling rate is increased by lowering the barrier V_{B1} (left-hand panel, highest left-hand dot rate).

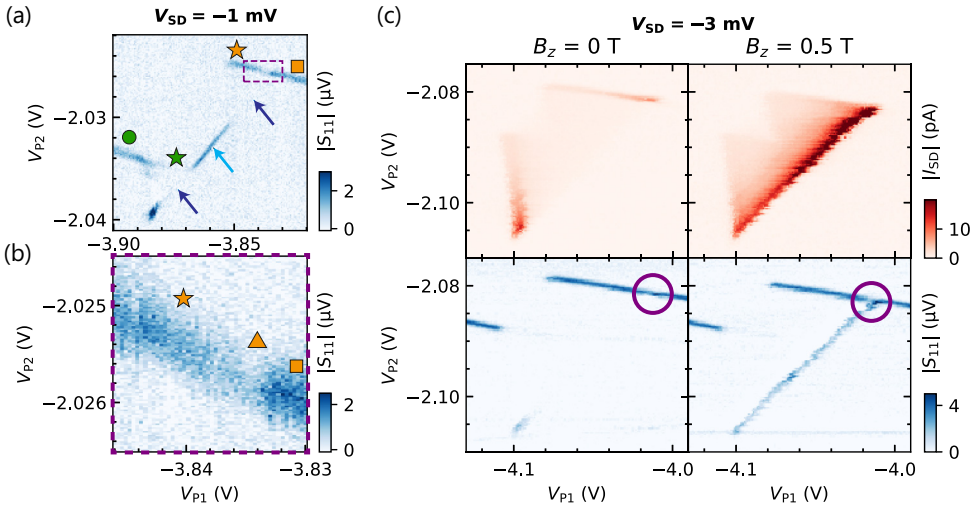

FIG. 8. Additional PSB data measured with a Si FinFET qubit device. (a) A dispersively sensed charge-stability map (showing the change in reflected amplitude $|S_{11}|$) of the FinFET device [29] near the $(2,0) \leftrightarrow (1,1)$ transition, as labeled, is shown with the different regimes indicated by yellow and green markers, following the definition in Fig. 3. At small bias, the two triple points are sufficiently separated to avoid overlap. The zero-detuning line (arrows) is visible outside the bias window (light-blue arrow) but disappears within the bias triangles (dark-blue arrows). As for the NW device, the dispersive PSB signature appears as a bright upper reservoir transition (yellow star) and an invisible lower reservoir transition (green star). Additionally, PSB is only weakly lifted close to zero detuning, leading to a minute gap in the upper reservoir transition (dashed purple rectangle). A higher-resolution scan of this region is shown in (b). The gap in the reservoir transition (orange triangle) is indicated, as well as the spin blockade (orange star) and the reservoir transition outside of the bias window (orange square). (c) The dc current (upper panels) through the FinFET shows the characteristic signature of PSB, as the current increases close to the triangle baseline when a magnetic field is applied (right panels). Unlike the Ge/Si NW DQD, the blockade remains largely intact in the inelastic cotunneling regime. Therefore, the reservoir transitions in the dispersive measurement (lower panels) remain largely unaffected, apart from a slight increase of the gap in the upper reservoir transition close to zero detuning (purple circles).

(dark blue arrows) the bias window in this charge-stability map. Evidently, the dynamics imposed by the bias voltage rearrange the population of the DQD states such that the triangle baselines disappear, while the interdot transition outside of the bias window remains very clearly visible.

Finally, the response of the dc current and the dispersive feature to a magnetic field is shown in Fig. 8(c) for a more negative bias $V_{SD} = -3\,\text{mV}$. Unlike for the Ge/Si NW device, PSB in the FinFETs is usually lifted by magnetic fields only close to zero detuning [15,40]. For this reason, the current at $B_z = 0.5$ T is high only at the triangle baselines, as inelastic processes only weakly lift PSB, leading to a small increase in current toward the top left. This is also reflected in the dispersively sensed data, where the upper reservoir transition largely prevails while the lower transition remains at low contrast. The slightly increasing gap in the upper transition close to zero detuning (purple circles) is consistent with the observation of enhanced current. Note that the first excited-state transition is not visible in these plots, as it lies at energies higher than the applied bias.

Overall, this observation highlights the broad impact of our finding, as the dispersive signature is present across different device platforms and material systems.

[1] W. Pauli, Über den Zusammenhang des Abschlusses der Elektronengruppen im Atom mit der Komplexstruktur der Spektren, Zeitsch. Phys. **31**, 765 (1925).
[2] K. Ono, D. G. Austing, Y. Tokura, and S. Tarucha, Current rectification by Pauli exclusion in a weakly coupled double quantum dot system, Science **297**, 1313 (2002).
[3] R. Li, F. E. Hudson, A. S. Dzurak, and A. R. Hamilton, Pauli spin blockade of heavy holes in a silicon double quantum dot, Nano Lett. **15**, 7314 (2015).
[4] N. W. Ashcroft and N. D. Mermin, *Solid State Physics* (Holt-Saunders, Philadelphia, 1976).
[5] D. Loss and D. P. DiVincenzo, Quantum computation with quantum dots, Phys. Rev. A **57**, 120 (1998).
[6] N. W. Hendrickx, W. I. L. Lawrie, M. Russ, F. van Riggelen, S. L. de Snoo, R. N. Schouten, A. Sammak, G. Scappucci, and M. Veldhorst, A four-qubit germanium quantum processor, Nature **591**, 580 (2021).
[7] S. G. J. Philips, M. T. Mądzik, S. V. Amitonov, S. L. de Snoo, M. Russ, N. Kalhor, C. Volk, W. I. L. Lawrie, D. Brousse, L. Tryputen, B. P. Wuetz, A. Sammak, M. Veldhorst, G. Scappucci, and L. M. K. Vandersypen, Universal control of a six-qubit quantum processor in silicon, Nature **609**, 919 (2022).
[8] A. J. Weinstein *et al.*, Universal logic with encoded spin qubits in silicon, Nature **615**, 817 (2023).

[9] S. Neyens *et al.*, Probing single electrons across 300-mm spin qubit wafers, Nature **629**, 80 (2024).
[10] T. Tanttu *et al.*, Assessment of the errors of high-fidelity two-qubit gates in silicon quantum dots, Nat. Phys. **20**, 1804 (2024).
[11] C. H. Yang, R. C. C. Leon, J. C. C. Hwang, A. Saraiva, T. Tanttu, W. Huang, J. C. Lemyre, K. W. Chan, K. Y. Tan, F. E. Hudson, K. M. Itoh, A. Morello, M. Pioro-Ladrière, A. Laucht, and A. S. Dzurak, Operation of a silicon quantum processor unit cell above one kelvin, Nature **580**, 350 (2020).
[12] L. Petit, H. G. J. Eenink, M. Russ, W. I. L. Lawrie, N. W. Hendrickx, S. G. J. Philips, J. S. Clarke, L. M. K. Vandersypen, and M. Veldhorst, Universal quantum logic in hot silicon qubits, Nature **580**, 355 (2020).
[13] J. Y. Huang *et al.*, High-fidelity spin qubit operation and algorithmic initialization above 1 K, Nature **627**, 772 (2024).
[14] M. J. Carballido, S. Svab, R. S. Eggli, T. Patlatiuk, P. Chevalier Kwon, J. Schuff, R. M. Kaiser, L. C. Camenzind, A. Li, N. Ares, E. P. A. M. Bakkers, S. Bosco, J. C. Egues, D. Loss, and D. M. Zumbühl, Compromise-free scaling of qubit speed and coherence, Nat. Commun. **16**, 7616 (2025).
[15] L. C. Camenzind, S. Geyer, A. Fuhrer, R. J. Warburton, D. M. Zumbühl, and A. V. Kuhlmann, A hole spin qubit in a fin field-effect transistor above 4 kelvin, Nat. Electron. **5**, 178 (2022).
[16] J. I. Colless, A. C. Mahoney, J. M. Hornibrook, A. C. Doherty, H. Lu, A. C. Gossard, and D. J. Reilly, Dispersive readout of a few-electron double quantum dot with fast rf gate sensors, Phys. Rev. Lett. **110**, 046805 (2013).
[17] M. F. Gonzalez-Zalba, S. Barraud, A. J. Ferguson, and A. C. Betz, Probing the limits of gate-based charge sensing, Nat. Commun. **6**, 6084 (2015).
[18] A. West, B. Hensen, A. Jouan, T. Tanttu, C.-H. Yang, A. Rossi, M. F. Gonzalez-Zalba, F. Hudson, A. Morello, D. J. Reilly, and A. S. Dzurak, Gate-based single-shot readout of spins in silicon, Nat. Nanotechnol. **14**, 437 (2019).
[19] M. Urdampilleta, D. J. Niegemann, E. Chanrion, B. Jadot, C. Spence, P.-A. Mortemousque, C. Bäuerle, L. Hutin, B. Bertrand, S. Barraud, R. Maurand, M. Sanquer, X. Jehl, S. D. Franceschi, M. Vinet, and T. Meunier, Gate-based high fidelity spin readout in a CMOS device, Nat. Nanotechnol. **14**, 737 (2019).
[20] A. Crippa, R. Ezzouch, A. Aprá, A. Amisse, R. Laviéville, L. Hutin, B. Bertrand, M. Vinet, M. Urdampilleta, T. Meunier, M. Sanquer, X. Jehl, R. Maurand, and S. De Franceschi, Gate-reflectometry dispersive readout and coherent control of a spin qubit in silicon, Nat. Commun. **10**, 2776 (2019).
[21] T. Lundberg, J. Li, L. Hutin, B. Bertrand, D. J. Ibberson, C.-M. Lee, D. J. Niegemann, M. Urdampilleta, N. Stelmashenko, T. Meunier, J. W. A. Robinson, L. Ibberson, M. Vinet, Y.-M. Niquet, and M. F. Gonzalez-Zalba, Spin quintet in a silicon double quantum dot: Spin blockade and relaxation, Phys. Rev. X **10**, 041010 (2020).
[22] M. S. Ferguson, L. C. Camenzind, C. Müller, D. E. F. Biesinger, C. P. Scheller, B. Braunecker, D. M. Zumbühl, and O. Zilberberg, Measurement-induced population switching, Phys. Rev. Res. **5**, 023028 (2023).
[23] D. Svastits, B. Hetényi, G. Széchenyi, J. Wootton, D. Loss, S. Bosco, and A. Pályi, Readout sweet spots for spin qubits with strong spin-orbit interaction, arXiv:2505.15878.
[24] S. D. Liles, F. Martins, D. S. Miserev, A. A. Kiselev, I. D. Thorvaldson, M. J. Rendell, I. K. Jin, F. E. Hudson, M. Veldhorst, K. M. Itoh, O. P. Sushkov, T. D. Ladd, A. S. Dzurak, and A. R. Hamilton, Electrical control of the *g* tensor of the first hole in a silicon MOS quantum dot, Phys. Rev. B **104**, 235303 (2021).
[25] S. Bosco, S. Geyer, L. C. Camenzind, R. S. Eggli, A. Fuhrer, R. J. Warburton, D. M. Zumbühl, J. C. Egues, A. V. Kuhlmann, and D. Loss, Phase-driving hole spin qubits, Phys. Rev. Lett. **131**, 197001 (2023).
[26] R. S. Eggli, S. Svab, T. Patlatiuk, D. A. Trüssel, M. J. Carballido, P. Chevalier Kwon, S. Geyer, A. Li, E. P. A. M. Bakkers, A. V. Kuhlmann, and D. M. Zumbühl, Cryogenic hyperabrupt strontium titanate varactors for sensitive reflectometry of quantum dots, Phys. Rev. Appl. **20**, 054056 (2023).
[27] M. G. House, I. Bartlett, P. Pakkiam, M. Koch, E. Peretz, J. van der Heijden, T. Kobayashi, S. Rogge, and M. Y. Simmons, High-sensitivity charge detection with a single-lead quantum dot for scalable quantum computation, Phys. Rev. Appl. **6**, 044016 (2016).
[28] N. Piot, B. Brun, V. Schmitt, S. Zihlmann, V. P. Michal, A. Apra, J. C. Abadillo-Uriel, X. Jehl, B. Bertrand, H. Niebojewski, L. Hutin, M. Vinet, M. Urdampilleta, T. Meunier, Y.-M. Niquet, R. Maurand, and S. D. Franceschi, A single hole spin with enhanced coherence in natural silicon, Nat. Nanotechnol. **17**, 1072 (2022).
[29] R. S. Eggli, T. Patlatiuk, E. G. Kelly, A. Orekhov, G. Salis, R. J. Warburton, D. M. Zumbühl, and A. V. Kuhlmann, Coupling a high-Q resonator to a spin qubit with all-electrical control, Phys. Rev. Res. **7**, 013197 (2025).
[30] M. G. House, T. Kobayashi, B. Weber, S. J. Hile, T. F. Watson, J. van der Heijden, S. Rogge, and M. Y. Simmons, Radio frequency measurements of tunnel couplings and singlet-triplet spin states in Si:P quantum dots, Nat. Commun. **6**, 8848 (2015).
[31] G. Zheng, N. Samkharadze, M. L. Noordam, N. Kalhor, D. Brousse, A. Sammak, G. Scappucci, and L. M. K. Vandersypen, Rapid gate-based spin read-out in silicon using an on-chip resonator, Nat. Nanotechnol. **14**, 742 (2019).
[32] T. Lundberg, D. J. Ibberson, J. Li, L. Hutin, J. C. Abadillo-Uriel, M. Filippone, B. Bertrand, A. Nunnenkamp, C.-M. Lee, N. Stelmashenko, J. W. A. Robinson, M. Vinet, L. Ibberson, Y.-M. Niquet, and M. F. Gonzalez-Zalba, Non-symmetric Pauli spin blockade in a silicon double quantum dot, npj Quantum Inf. **10**, 28 (2024).
[33] S. Geyer, B. Hetényi, S. Bosco, L. C. Camenzind, R. S. Eggli, A. Fuhrer, D. Loss, R. J. Warburton, D. M. Zumbühl, and A. V. Kuhlmann, Anisotropic exchange interaction of two hole-spin qubits, Nat. Phys. **20**, 1152 (2024).
[34] D. Jirovec, P. M. Mutter, A. Hofmann, A. Crippa, M. Rychetsky, D. L. Craig, J. Kukucka, F. Martins, A. Ballabio, N. Ares, D. Chrastina, G. Isella, G. Burkard, and G. Katsaros, Dynamics of hole singlet-triplet qubits with large *g*-factor differences, Phys. Rev. Lett. **128**, 126803 (2022).
[35] F. N. M. Froning, M. J. Rančić, B. Hetényi, S. Bosco, M. K. Rehmann, A. Li, E. P. A. M. Bakkers, F. A. Zwanenburg,

D. Loss, D. M. Zumbühl, and F. R. Braakman, Strong spin-orbit interaction and g-factor renormalization of hole spins in Ge/Si nanowire quantum dots, Phys. Rev. Res. **3**, 013081 (2021).

[36] J. Xiang, W. Lu, Y. Hu, Y. Wu, H. Yan, and C. M. Lieber, Ge/Si nanowire heterostructures as high-performance field-effect transistors, Nature **441**, 489 (2006).

[37] X.-J. Hao, T. Tu, G. Cao, C. Zhou, H.-O. Li, G.-C. Guo, W. Y. Fung, Z. Ji, G.-P. Guo, and W. Lu, Strong and tunable spin-orbit coupling of one-dimensional holes in Ge/Si core/shell nanowires, Nano Lett. **10**, 2956 (2010).

[38] S. Conesa-Boj, A. Li, S. Koelling, M. Brauns, J. Ridderbos, T. T. Nguyen, M. A. Verheijen, P. M. Koenraad, F. A. Zwanenburg, and E. P. A. M. Bakkers, Boosting hole mobility in coherently strained [110]-oriented Ge-Si core-shell nanowires, Nano Lett. **17**, 2259 (2017).

[39] F. N. M. Froning, M. K. Rehmann, J. Ridderbos, M. Brauns, F. A. Zwanenburg, A. Li, E. P. A. M. Bakkers, D. M. Zumbühl, and F. R. Braakman, Single, double, and triple quantum dots in Ge/Si nanowires, Appl. Phys. Lett. **113**, 073102 (2018).

[40] S. Geyer, L. C. Camenzind, L. Czornomaz, V. Deshpande, A. Fuhrer, R. J. Warburton, D. M. Zumbühl, and A. V. Kuhlmann, Self-aligned gates for scalable silicon quantum computing, Appl. Phys. Lett. **118**, 104004 (2021).

[41] M. Urdampilleta, A. Chatterjee, C. C. Lo, T. Kobayashi, J. Mansir, S. Barraud, A. C. Betz, S. Rogge, M. F. Gonzalez-Zalba, and J. J. L. Morton, Charge dynamics and spin blockade in a hybrid double quantum dot in silicon, Phys. Rev. X **5**, 031024 (2015).

[42] A. P. Higginbotham, F. Kuemmeth, T. W. Larsen, M. Fitzpatrick, J. Yao, H. Yan, C. M. Lieber, and C. M. Marcus, Antilocalization of Coulomb blockade in a Ge/Si nanowire, Phys. Rev. Lett. **112**, 216806 (2014).

[43] S. Roddaro, A. Fuhrer, P. Brusheim, C. Fasth, H. Q. Xu, L. Samuelson, J. Xiang, and C. M. Lieber, Spin states of holes in Ge/Si nanowire quantum dots, Phys. Rev. Lett. **101**, 186802 (2008).

[44] M. Brauns, J. Ridderbos, A. Li, E. P. A. M. Bakkers, and F. A. Zwanenburg, Electric-field dependent g-factor anisotropy in Ge-Si core-shell nanowire quantum dots, Phys. Rev. B **93**, 121408(R) (2016).

[45] A. Zarassi, Z. Su, J. Danon, J. Schwenderling, M. Hocevar, B. M. Nguyen, J. Yoo, S. A. Dayeh, and S. M. Frolov, Magnetic field evolution of spin blockade in Ge/Si nanowire double quantum dots, Phys. Rev. B **95**, 155416 (2017).

[46] C. Kloeffel, M. Trif, and D. Loss, Strong spin-orbit interaction and helical hole states in Ge/Si nanowires, Phys. Rev. B **84**, 195314 (2011).

[47] C. Kloeffel, M. J. Rančić, and D. Loss, Direct Rashba spin-orbit interaction in Si and Ge nanowires with different growth directions, Phys. Rev. B **97**, 235422 (2018).

[48] J. H. Ungerer, P. Chevalier Kwon, T. Patlatiuk, J. Ridderbos, A. Kononov, D. Sarmah, E. P. A. M. Bakkers, D. Zumbühl, and C. Schönenberger, Charge-sensing of a Ge/Si core/shell nanowire double quantum dot using a high-impedance superconducting resonator, Mater. Quantum. Technol. **3**, 031001 (2023).

[49] P. Apostolidis, B. J. Villis, J. F. Chittock-Wood, J. M. Powell, A. Baumgartner, V. Vesterinen, S. Simbierowicz, J. Hassel, and M. R. Buitelaar, Quantum paraelectric varactors for radiofrequency measurements at millikelvin temperatures, Nat. Electron. **7**, 760 (2024).

[50] J. Schuff, M. J. Carballido, M. Kotzagiannidis, J. C. Calvo, M. Caselli, J. Rawling, D. L. Craig, B. van Straaten, B. Severin, F. Fedele, S. Svab, P. C. Kwon, R. S. Eggli, T. Patlatiuk, N. Korda, D. Zumbühl, and N. Ares, Fully autonomous tuning of a spin qubit, Nat. Electron. (2026).

[51] J. Danon and Y. V. Nazarov, Pauli spin blockade in the presence of strong spin-orbit coupling, Phys. Rev. B **80**, 041301(R) (2009).

[52] F. N. M. Froning, M. J. Rančić, B. Hetényi, S. Bosco, M. K. Rehmann, A. Li, E. P. A. M. Bakkers, F. A. Zwanenburg, D. Loss, D. M. Zumbühl, and F. R. Braakman, Strong spin-orbit interaction and g-factor renormalization of hole spins in Ge/Si nanowire quantum dots, Phys. Rev. Res. **3**, 013081 (2021).

[53] A. C. Johnson, J. R. Petta, C. M. Marcus, M. P. Hanson, and A. C. Gossard, Singlet-triplet spin blockade and charge sensing in a few-electron double quantum dot, Phys. Rev. B **72**, 165308 (2005).

[54] N. Shaji, C. B. Simmons, M. Thalakulam, L. J. Klein, H. Qin, H. Luo, D. E. Savage, M. G. Lagally, A. J. Rimberg, R. Joynt, M. Friesen, R. H. Blick, S. N. Coppersmith, and M. A. Eriksson, Spin blockade and lifetime-enhanced transport in a few-electron Si/SiGe double quantum dot, Nat. Phys. **4**, 540 (2008).

[55] F. Qassemi, W. A. Coish, and F. K. Wilhelm, Stationary and transient leakage current in the Pauli spin blockade, Phys. Rev. Lett. **102**, 176806 (2009).

[56] N. S. Lai, W. H. Lim, C. H. Yang, F. A. Zwanenburg, W. A. Coish, F. Qassemi, A. Morello, and A. S. Dzurak, Pauli spin blockade in a highly tunable silicon double quantum dot, Sci. Rep. **1**, 110 (2011).

[57] W. A. Coish and F. Qassemi, Leakage-current line shapes from inelastic cotunneling in the Pauli spin blockade regime, Phys. Rev. B **84**, 245407 (2011).

[58] V. N. Golovach and D. Loss, Transport through a double quantum dot in the sequential tunneling and cotunneling regimes, Phys. Rev. B **69**, 245327 (2004).

[59] R. Hanson, L. P. Kouwenhoven, J. R. Petta, S. Tarucha, and L. M. K. Vandersypen, Spins in few-electron quantum dots, Rev. Mod. Phys. **79**, 1217 (2007).

[60] F. Vigneau, F. Fedele, A. Chatterjee, D. Reilly, F. Kuemmeth, F. Gonzalez-Zalba, E. Laird, and N. Ares, Probing quantum devices with radio-frequency reflectometry, Appl. Phys. Rev. **10**, 021305 (2023).

[61] N. Hendrickx, D. Franke, A. Sammak, G. Scappucci, and M. Veldhorst, Fast two-qubit logic with holes in germanium, Nature **577**, 487 (2020).

[62] A. C. Betz, R. Wacquez, M. Vinet, X. Jehl, A. L. Saraiva, M. Sanquer, A. J. Ferguson, and M. F. Gonzalez-Zalba, Dispersively detected Pauli spin-blockade in a silicon nanowire field-effect transistor, Nano Lett. **15**, 4622 (2015).

[63] R. Mizuta, R. M. Otxoa, A. C. Betz, and M. F. Gonzalez-Zalba, Quantum and tunneling capacitance in charge and spin qubits, Phys. Rev. B **95**, 045414 (2017).

[64] P. Pakkiam, A. V. Timofeev, M. G. House, M. R. Hogg, T. Kobayashi, M. Koch, S. Rogge, and M. Y. Simmons, Single-shot single-gate rf spin readout in silicon, Phys. Rev. X **8**, 041032 (2018).

[65] A. Russell, A. Zotov, R. Zhao, A. S. Dzurak, M. F. Gonzalez-Zalba, and A. Rossi, Gate-based spin readout of hole quantum dots with site-dependent *g*-factors, Phys. Rev. Appl. **19**, 044039 (2023).

[66] S. Schaal, I. Ahmed, J. A. Haigh, L. Hutin, B. Bertrand, S. Barraud, M. Vinet, C.-M. Lee, N. Stelmashenko, J. W. A. Robinson, J. Y. Qiu, S. Hacohen-Gourgy, I. Siddiqi, M. F. Gonzalez-Zalba, and J. J. L. Morton, Fast gate-based readout of silicon quantum dots using Josephson parametric amplification, Phys. Rev. Lett. **124**, 067701 (2020).

[67] Simon Svab, Supporting data for a direct dispersive signature of Pauli spin blockade (2025), https://doi.org/10.5281/zenodo.15746571.

[68] E. G. Kelly, A. Orekhov, N. W. Hendrickx, M. Mergenthaler, F. J. Schupp, S. Paredes, R. S. Eggli, A. V. Kuhlmann, P. Harvey-Collard, A. Fuhrer, and G. Salis, Capacitive crosstalk in gate-based dispersive sensing of spin qubits, Appl. Phys. Lett. **123**, 262104 (2023).